Microscopic Characterization of Uranium Nitrides Synthesized by Oxidative Ammonolysis of Uranium Tetrafluoride

G. W. Chinthaka Silva,[†] Charles B. Yeamans,[‡] Longzhou Ma,[†] Gary S. Cerefice,[†] Kenneth R. Czerwinski,*[,†] and Alfred P. Sattelberger[†,§]

University of Nevada, Las Vegas, Harry Reid Center for Environmental Studies, Box 454009, 4505 Maryland Parkway, Las Vegas, Nevada 89154, University of California, Berkeley, Department of Nuclear Engineering, 4155 Etcheverry Hall, M.C. 1730, Berkeley, California 94720-1730, and Energy Sciences and Engineering Directorate, Argonne National Laboratory, 9700 Cass Avenue, Argonne, Illinois 60439

Received November 27, 2007. Revised Manuscript Received March 7, 2008

The oxidative ammonolysis route was used to synthesize three uranium nitrides, UN_2, U_2N_3, and UN, using UF_4 as the starting material. Powder XRD analysis showed the UN_2 and U_2N_3 products to contain less than 1.0 wt % uranium oxides. UO_2 level was identified to be 5.0 (0) wt % in the UN product as it is made, but this level increases upon exposure to air. The morphology of these nitrides was studied with SEM, while the microstructures of UN_2 and U_2N_3 were investigated by TEM techniques for the first time. An explicit microstructural characterization of UN is also presented. These characterizations showed that UN has a long-range order in its structure and bulk of the UO_2 impurities present on the UN microparticle surface, likely originating from minute oxygen impurities in the inert atmosphere cover gas and/or diffusion through the quartz reactor tube at high temperatures. Surface area measurements demonstrated a 10-fold increase in surface area during the ammonolysis step, from 0.03 to 0.26 m^2/g, and minimal change during the denitriding step.

1. Introduction

Uranium(III) mononitride (UN) has a number of favorable nuclear fuel properties when compared to uranium oxide, including high fissile atom density, high melting point, and high thermal conductivity.[1] As a result, UN is receiving attention as a potential fuel for next-generation nuclear power systems. In nuclear fuel applications, pellets of a nitride, oxide, carbide, or other actinide compounds are sintered from a powder starting material. The pronounced influence of particle size, morphology, and surface area on the nuclear fuel properties of the final sintered pellet[2] provides the motivation for characterization of the starting powders.

Carbothermic reduction has been used extensively to synthesize nitride fuel material.[3] In the carbothermic reduction/nitrification process, metal oxides are mixed with stoichiometric or excess amounts of carbon and then annealed at 1600−1700 °C in an atmosphere of N_2 or N_2/H_2. The carbothermic process faces challenges in producing a high-density product free of oxide and carbide impurities.[4–6] For mixed actinide fuel materials, these problems are further compounded by the need to incorporate americium into the fuel matrix. Americium has a sufficiently high vapor pressure at the temperatures used during the carbothermic process[7] to cause volatilization loss and contamination problems when synthesizing mixed actinide nitrides.[8]

Alternate routes for the synthesis of uranium nitrides have been previously explored, including conversion of the metal hydride or metal directly to the nitride under nitrogen gas,[9] ammonolysis of the metal or metal carbide to the nitride,[10] and ammonolysis of the metal fluoride.[11] Ammonolysis of the metal fluoride is particularly interesting due to the significant reductions in process temperatures required to convert the metal oxides to the nitride compared to the carbothermic reduction route. In the low-temperature fluoride oxidative ammonolysis route, UF_4 is reacted with an atmosphere of gaseous ammonia to form uranium(VI) dinitride (UN_2).[11,12] The dinitride can be reduced to uranium sesquinitride (U_2N_3) and UN under inert atmosphere from 700 to 1100 °C.[13]

Uranium nitrides have been characterized by many techniques: X-ray powder diffraction, neutron powder diffrac-

* To whom correspondence should be addressed. Phone: (702) 895 0501. Fax: (702) 895 3094. E-mail czerwin2@unlv.nevada.edu.
[†] University of Nevada.
[‡] University of California.
[§] Argonne National Laboratory.

(1) Streit, M.; Ingold, F. *J. Eur. Ceram. Soc.* **2005**, *25*, 2687.
(2) Cordfunke, E. H. P.; van der Giessen, A. A. *J. Nucl. Mater.* **1967**, *24*, 141.
(3) Arai, Y.; Fukushima, S.; Shiozawa, K.; Handa, M. *J. Nucl. Mater.* **1989**, *168*, 280.
(4) Mukerjee, S. K.; Dehadraya, J. V.; Vaidya, V. N.; Sood, D. D. *J. Nucl. Mater.* **1991**, *185*, 39.
(5) Minato, K.; Akabori, M.; Takano, M.; Arai, Y.; Nakajima, K.; Itoh, A.; Ogawa, T. *J. Nucl. Mater.* **2003**, *320*, 18.
(6) McLaren, J. R.; Atkinson, P. W. M. *J. Nucl. Mater.* **1965**, *17*, 142.
(7) Ward, J. W.; Kleinschmidt, P. D.; Haire, R. G. *J. Chem. Phys.* **1979**, *71*, 3920.
(8) Ogawa, T.; Shirasu, Y.; Minato, K.; Serizawa, H. *J. Nucl. Mater.* **1997**, *247*, 151.
(9) Anselin, F. CEA report R.2988, 1965.
(10) Katsura, M.; Hirota, M.; Miyake, M. *J. Alloys Compd.* **1994**, *213/214*, 440.
(11) Yeamans, C. B.; Silva, G. W. C.; Cerefice, G. S.; Czerwinski, K. R.; Hartmann, T.; Burrell, A. K.; Sattelberger, A. P. *J. Nucl. Mater.* **2008**, *347*, 75–78.
(12) Funk, H.; Böhland, H. *Z. Anorg. Allg. Chem.* **1964**, *334*, 155.
(13) Evans, P. E.; Davies, T. J. *J. Nucl. Mater.* **1963**, *10*, 42.
(14) Mueller, M. H.; Knott, H. W. *Acta Crystallogr.* **1958**, *11*, 751.
(15) Kuznietz, M. *Phys. Rev.* **1969**, *180*, 476.

10.1021/cm7033646 CCC: $40.75
Published on Web 04/12/2008

tion,[14] nuclear magnetic resonance,[15] transmission electron microscopy,[16,17] and X-ray photoelectron spectroscopy.[18] The compounds UN_2, U_2N_3, and UN are the common nitrides of uranium[19] and have unique crystallographic properties that can be used to differentiate one from another. The UN_2 compound has a CaF_2-type face-centered cubic lattice with a lattice parameter of 0.531(1) nm,[20] while UN is a NaCl-type face-centered cubic lattice with a cubic lattice parameter of 0.48880(1) nm when pure.[21] The lattice parameter of UN is sensitive to carbon impurities[22] and insensitive to small oxygen impurities.[23] Both UN_2 and UN are indexed in the *Fm*3*m* space group (#225). The U_2N_3 compound is body-centered cubic with a cubic lattice parameter of 1.0678(5) nm and indexed in the $Ia\bar{3}$ space group. Uranium nitrides form a continuous phase between the dinitride and the sesquinitride. Lattice parameters and the resulting X-ray densities vary over that range, depending on the exact stoichiometry. The lattice parameter of $UN_{1.5 \le x<2}$ can vary over a fairly wide range: 1.0678(5) nm for precisely stoichiometric $UN_{1.5}$, 1.0580(5) nm for $UN_{1.75}$,[24,25] up to the values for UN_2.

Previous microscopy studies [5,16,17] have focused primarily on sintered pellets of UN. The work of Le et al.[16] and Sole and Van der Walt[17] reports the TEM characterization of UN specimens prepared using ion thinning and electropolishing. Samples for the current study were prepared using a solution-drop method, which does not introduce artifacts or deposits, and microtome cutting method, which can produce samples with a thickness under 25 nm.[26] Microtome cutting has been found to produce high-quality TEM sample specimens in observing the cross-sectional as well as microstructural characterization.[26] Uranium nitride samples prepared by microtome cutting permit detailed examination of morphology and microstructure of uranium nitride samples. Because microcrystalline properties influence the sinterability of UN and a fuel-quality sintered UN pellet is the ultimate goal of any nitride fabrication process for nuclear fuel, it is important to characterize the starting nitride material in sufficient detail. The quantity and consistency of oxide impurities affects the microscale and nanoscale morphology of UN, which ultimately determines the quality of the final sintered pellet[17] necessitating characterization of oxide species in the nitride matrix.

In this work, the low-temperature fluoride route was used to synthesize UN_2, U_2N_3, and UN, whose phase purity and morphology was then examined by powder XRD and SEM/TEM, respectively. This work reports for the first time the microstructures of UN_2 and U_2N_3 examined by TEM. The microstructural characterization of UN is also presented and predicts the location of UO_2 impurity phase in the nitride matrix based on the results of the microparticles that have been investigated by TEM. The relative concentration of uranium species in the solids were determined by Rietveld analysis of the X-ray powder diffraction patterns. Surface area measurements of the fluoride and nitride species are presented as an indication of the sinterability and surface reactivity of the material and to track the microstructural changes during the ammonolysis step.

2. Experimental Details

2.1. Synthesis of Uranium Nitrides. The direct ammonolysis of UF_4 was used to synthesize UN_2. A 1015.8 mg batch of UF_4 (International Bio-Analytical Industries, Inc.) was loaded in a quartz boat wrapped with platinum foil and placed inside a 25.4 mm diameter quartz tube, capped on either end with 25 mm quartz Solv-Seal fittings (Andrews Glass Co., Inc.). Pyrex Solv-Seal caps fitted with 15 mm high-vacuum Teflon stopcocks sealed the tube and allowed a controlled atmosphere to blanket the sample. The sample was held at 800 °C for 60 min under ammonia gas (research grade, Praxair), after which 858.5 mg of UN_2 was obtained. A 218.7 mg batch of U_2N_3 was synthesized by heating 225.4 mg of the synthesized UN_2 under an inert atmosphere (ultra-high-purity argon, 99.9999%, Praxair) at 700 °C for 60 min. A separate 35.8 mg UN_2 sample was heated to 1100 °C for 30 min under an inert atmosphere producing 34.0 mg of UN.

2.2. Characterization Methods. *2.2.1. XRD.* X-ray powder diffraction (XRD) patterns were obtained at the department of Geoscience of University of Nevada, Las Vegas using a Philips PANalytical X'Pert Pro instrument with a Cu Kα target and a Ni filter, using 40 mA current and 40 kV tension. Phase composition was determined using the following reference patterns from the International Center for Diffraction Data: UN_2 (01-073-1713), U_2N_3 (01-073-1712), UN (00-032-1397), and UO_2 (00-041-1422). A lanthanum hexaboride internal standard (SRM 660a) was admixed with the uranium nitride samples before acquisition of the XRD powder patterns in order to perform Rietveld analysis[27] on the experimental XRD patterns to determine cubic lattice parameters and X-ray densities of each nitride sample. Instrumental parameters were optimized with the XRD pattern obtained for the internal standard by utilizing the reference ICDD pattern number 00-034-0427.

2.2.2. Surface Area Analysis. Surface area analysis (SAA) was performed on a Quantachrome Nova 1000, which uses the Brunauer–Emmett–Teller method.[28] Nitrogen is used as the adsorbing gas at a working pressure below 100 kPa. No reactions with any compounds occurred during the experiment within the SAA working temperature range of 77–310 K. To avoid potential thermal decomposition or oxidation, samples were degassed at ambient laboratory temperature of 298–310 K.

2.2.3. Microscopy. The morphology of the nitride samples was studied by scanning electron microscopy (SEM) and transmission electron microscopy (TEM). The SEM imaging was performed on a JEOL scanning electron microscope model JSM-5610 equipped with secondary electron (SE) and backscattered electron (BE) detectors and an Oxford ISIS EDS (energy-dispersive spectrometer)

(16) Le, T. N.; Lorenzelli, N.; Zuppiroli, L. *J. Nucl. Mater.* **1991**, *184*, 230.
(17) Sole, M. J.; Van der Walt, C. M. *Acta Metall.* **1968**, *16*, 501.
(18) Black, L.; Miserque, F.; Gouder, T.; Havela, L.; Rebizant, J.; Wastin, F. *J. Alloys Compd.* **2001**, *315*, 36.
(19) Morss, L. R.; Edelstein, N. M.; Fuger, J., Eds. *The Chemistrty of the Actinides and Transactinide Elements*, 3rd ed.; Springer Press: New York, 2006; Vol. 1.
(20) Rundle, R. E.; Baenziger, N. C.; Wilson, A. S.; McDonald, R. A. *J. Am. Chem. Soc.* **1948**, *70*, 99.
(21) Cordfunke, E. H. P. *J. Nucl. Mater.* **1975**, *56*, 319.
(22) Leitnaker, J. M.; Potter, R. A.; Spear, K. E.; Laing, W. R. *High Temp. Sci.* **1969**, *1*, 389.
(23) Muromura, T.; Tagawa, H. *J. Nucl. Mater.* **1979**, *79*, 264.
(24) Tagawa, H. *J. Nucl. Mater.* **1974**, *51*, 78.
(25) Tagawa, H.; Masaki, N. *J. Inorg. Chem.* **1974**, *26*, 1099.
(26) Silva, G. W. C.; Ma, L.; Hemmers, O.; Lindle, D. *Micron* **2008**, *39*, 269.
(27) Reitveld, H. M. *J. Appl. Crystallogr.* **1969**, *2*, 65.
(28) Brunauer, S.; Emmitt, P. H.; Teller, E. *J. Am. Chem. Soc.* **1938**, *60*, 309.

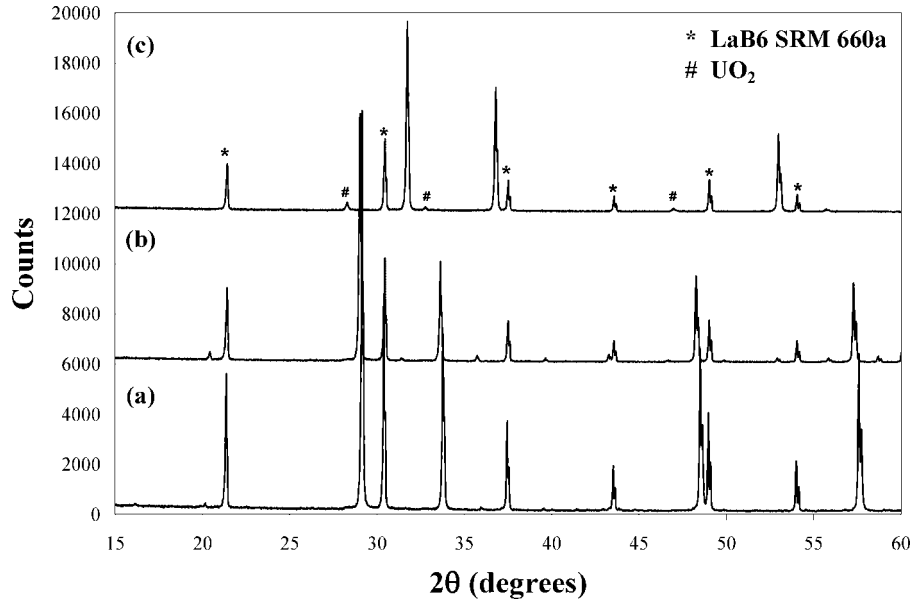

Figure 1. Experimental XRD patterns of the synthesized uranium nitrides: (a) UN_2, (b) U_2N_3, and (c) UN.

system with an acceleration voltage of 15 kV. Gold-coated powder samples mounted on double-sided carbon tapes were used to investigate the bulk particle morphology of the samples using the SE imaging mode of SEM. A JEOL electron probe microanalyzer model JXA-8900 equipped with four wavelength-dispersive X-ray spectrometers and an EDS was used to quantitatively analyze the elemental distributions in the samples.

A Tecnai-G2-F30 supertwin transmission electron microscope system with a 300 keV Schottky field emission gun was used to characterize the samples. Bulk morphology was analyzed using the conventional bright field (BF) mode, and lattice structure was analyzed using the high-resolution TEM (HRTEM) mode. All TEM images were recorded using a slow scan CCD camera attached to a Gatan GIF 2000 energy filter. Web-based kinematical electron diffraction and HRTEM simulations[29] were used in analyzing and confirming the HRTEM imaging of the samples. The elemental distribution of each sample was also determined using the corresponding X-ray energy-dispersive spectrometry (XEDS) under the STEM mode (scanning transmission electron microscopy) condition.

2.3. TEM Specimen Preparation. Two techniques were used for TEM specimen preparation: solution-drop and microtome cutting. The solution-drop method was utilized to explore the morphology of the nitrides samples. Microtome cutting was used to prepare samples for cross-section analysis and HRTEM imaging.

To prepare samples by the solution-drop method, 1−5 mg of the sample material was ground by hand in a mortar and pestle and added to 5.0 mL of reagent-grade methanol. This mixture was agitated in an ultrasonic water bath for 5 min to form a homogeneous colloidal suspension. One drop of the suspension was placed onto a 3 mm diameter carbon-coated copper grid using a small-tipped transfer pipet. The solution was evaporated from the sample at room temperature, leaving the fine particulate sample deposited on the carbon film, which was then used in the TEM observation.

For the microtome cutting method, several milligrams of sample were mixed with spur resin[26] in a microvial, which was then solidified by drying at 60 °C overnight. The spur resin used for these samples was a mixture of 10.0 g of ERL (vinylcyclohexene dioxide), 4.0 g of DER (a diglycidyl ether of polypropylene glycol), 26.0 g of NSA (nonenyl succinic anhydride), and 0.4 g of DMAE (dimethylaminoethanol). The sample embedded in the resin was cut into slices with a thickness of 20−50 nm using a Leica EM UC6rt microtome. The resulting samples were loaded onto a 3 mm copper grid for TEM analysis.

3. Results

3.1. Chemical Analysis Using XRD and Electron Microprobe. Powder XRD patterns of the UN_2, U_2N_3, and UN samples are shown in Figure 1, and the narrow, well-defined, high-intensity peaks indicate these samples are decidedly crystalline.[30] On the basis of the Rietveld analysis applied to the XRD patterns, the as-synthesized UN_2 sample consisted of a 0.6 (3) wt % secondary oxide phase. There are also peaks in the UN_2 spectrum at 20.2° and 36.1° 2theta values (Figure 1a) that have some resemblance to the peaks identified in the U_2N_3 XRD pattern (Figure 1b) but are not accounted for by the UN_2 structure. In order to investigate these peaks further, another UN_2 sample was synthesized under the same NH_3 atmosphere and temperature (800 °C) for 390 min. The Rietveld analyses of the sample held at this temperature for 60 min and the sample held for 390 min are shown in Figure 2a and 2b, respectively. The peaks at 20.2° and 36.1° 2theta values have disappeared for the sample made after heating for 390 min. Incomplete conversion, with the material still slightly substoichiometric UN_2, could account for these peaks since UN_2 and U_2N_3 are known to have a wide range of continuous stoichiometry[24,25] and supersymmetries that cause weak reflections to appear in the XRD pattern. The UN sample was determined to consist of two chemical phases, the primary UN phase and a 5.0 (1) wt % UO_2 impurity phase. Table 1 shows the cubic lattice parameters determined using Rietveld refinement and X-ray densities of each nitride calculated from the experimental XRD patterns, along with published values of each nitride

(29) Zuo, J. M.; Mabon, J. C. Web-based Electron Microscopy Application Software: Web-EMAPS. *Microsc. Microanal.* **2004**, *10* (Suppl 2); URL: http://emaps.mrl.uiuc.edu/.

(30) Jenkins, R.; Synder, R. L. *Introduction to X-ray powder Diffractometry*; John Wiley & Sons, Inc.: New York, 1996; Vol. 138.

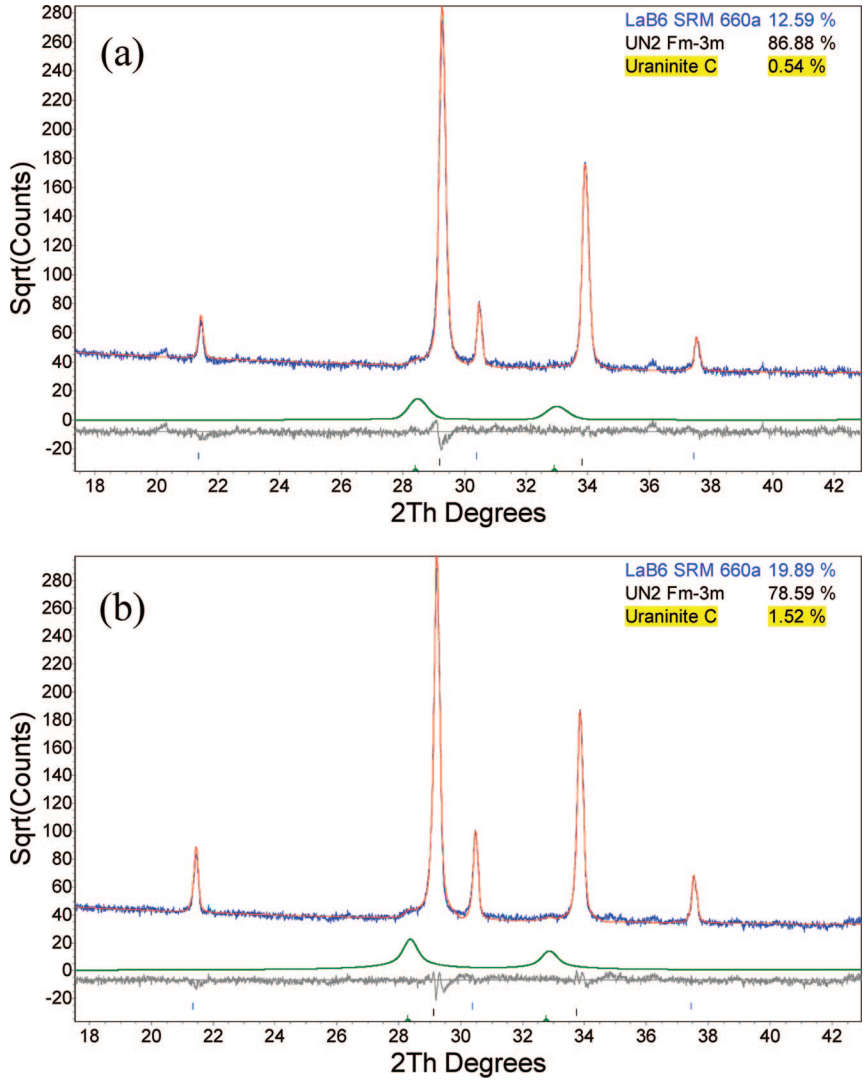

Figure 2. Rietveld analysis of UN_2 samples showing the impurity peaks in the low 2theta angles: (a) synthesized by heating UF_4 at 800 °C for 1 h, (b) synthesized by heating at 800 °C for 6.5 h. Experimental pattern is blue, the fit is red, while the difference curve is gray. The green-colored pattern shows the UO_2 match.

Table 1. Lattice Parameters and X-ray Phase Densities of the Uranium Nitrides Calculated from Experimental Patterns Using Rietveld Analysis

	lattice parameter (nm)		X-ray phase density (g cm^{-3})	
sample	calcd	ref	calcd	ref 20
UN_2	0.53027(1)	0.531(1)[20]	11.8516(2)	11.73
U_2N_3	1.06691(1)	1.0678–1.0580(5)[20,25]	11.3340(2)	11.24
UN	0.48899(1)	0.48899(2)[21]	14.3175(5)	14.32

Table 2. Elemental Compositions Determined by Electron Microprobe Studies

	elemental %		
sample	U	N	O
UN_2	89.02 ± 1.72	10.68 ± 0.20	0.29 ± 0.38
U_2N_3	90.77 ± 1.64	8.26 ± 0.10	0.97 ± 0.30
UN	93.17 ± 1.94	5.14 ± 0.13	1.69 ± 0.41

Table 3. Measured Surface Areas

sample	surface area (m^2/g)
UF_4	0.03 (3)
UN_2	0.26 (3)
U_2N_3	0.26 (3)
UN	0.23 (3)

system. The variable stoichiometry of the $UN_{1.5 \le x<2}$ phase likely leads to the departure from the pure compound lattice parameter and density for synthesized U_2N_3 and UN_2.

Electron microprobe determination showed that there are considerable amounts of oxygen impurities in U_2N_3 and UN (Table 2) and confirms the presence of UO_2 as the secondary phase. The oxygen level is highest in UN and lowest in UN_2. The error in the oxygen quantity measurement for UN_2 sample is large because the oxygen level is near the lower detectable limit of this technique.

3.2. Surface Area Analysis. Surface area analysis showed a 10-fold increase upon ammonolysis of UF_4 to UN_2. The surface area of the starting UF_4 sample was well below the specified reliable detection limit of the instrument, but the measurement was found to be repeatable with sufficient sample. Measured surface areas of the starting material and all nitrides formed are shown in Table 3.

3.3. Microscopy of UN_2. The SE-SEM image of the UN_2 sample (Figure 3) shows the UN_2 particles are primarily irregular grains with some discrete flat faces. The observed particle characteristic length distribution ranges from 0.1 to

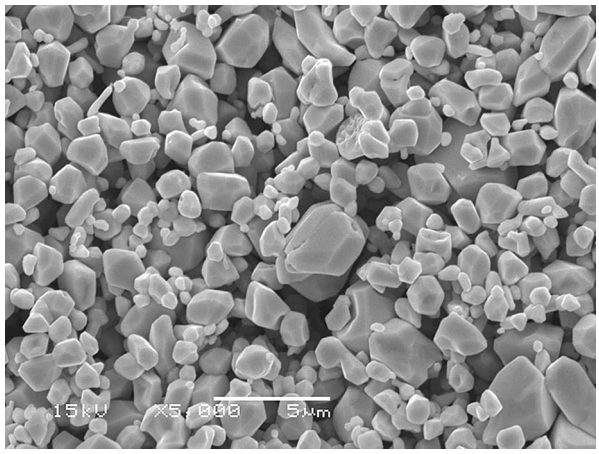

Figure 3. SE-SEM micrograph of UN_2.

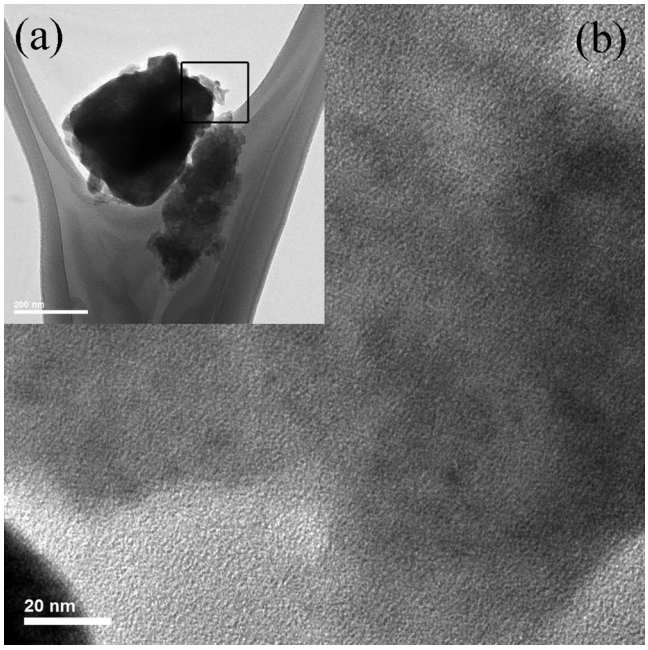

Figure 4. TEM BF images of UN_2 particles.

6 μm, with incompletely crystallized particle faces making it difficult to measure the particle sizes accurately.

The TEM image of the UN_2 specimen prepared using the solution-drop method (Figure 4a) shows several agglomerated particles. Because they reside as aggregates, it is difficult to identify any particular shape of the UN_2 particles using this sample preparation technique. The characteristic lengths of the particles in the TEM images (150–450 nm) are in the lower range of the length distribution identified in the SEM imaging (100–6000 nm) because of the higher magnification attainable with TEM imaging. A higher magnification TEM BF image of the edge of the particle (Figure 4b) shows no detectable precipitates, defects, or faceted surfaces, indicating that the focus area of the particle does not have detectable impurity phases.

Figure 5a is the cross-sectional TEM BF image of another UN_2 particle, used to obtain the SAD pattern in Figure 5b. Most of the major electron diffraction spots in this SAD pattern correspond to the diffraction of UN_2 in the {111} direction in reciprocal space under [011] zone axis. Most of the other diffraction spots due to UN_2 are not indexed for

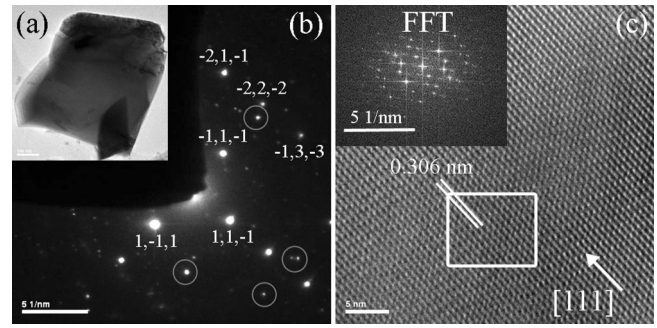

Figure 5. UN_2 micrographs: (a) TEM BF image, (b) SAD pattern in [011] zone, (c) HRTEM image.

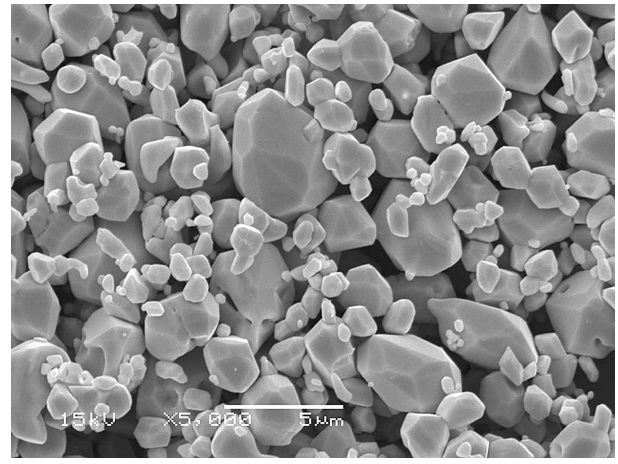

Figure 6. SE-SEM micrograph of U_2N_3.

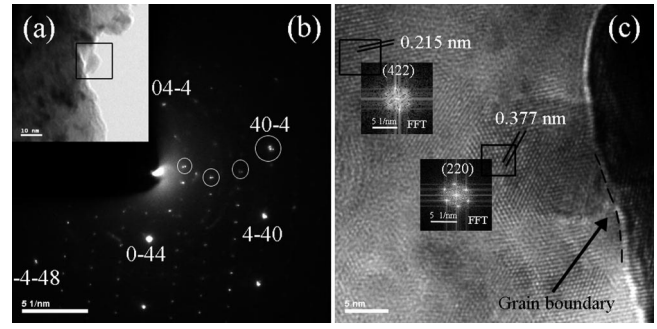

Figure 7. TEM images of U_2N_3: (a) TEM BF image, (b) SAD pattern in [111] zone axis, (c) HRTEM image. The HRTEM image shows a grain boundary in the focused area of the particle, which can cause the extra weak diffractions observed in the SAD pattern.

reasons of figure clarity. The diffraction spots circled could be due to minor secondary phases such as UO_2, and the weak diffractions in the background of the SAD pattern are probably due to polycrystallinity within the focused particle area. The lattice fringes in the HRTEM image in Figure 5c correspond to the interplanar d spacing of UN_2 unit cell in (111) projection (for UN_2 $d_{111} = 0.30657$ nm[20]).

3.4. Microscopy of U_2N_3. The SE-SEM image of U_2N_3 sample particles (Figure 6) shows a similar morphology to that of the UN_2 sample: irregular grains with incompletely crystallized faces. The particle sizes range from 0.1 to 6 μm, also similar to the UN_2 sample.

The TEM BF image of a microtome cut U_2N_3 sample is shown in Figure 7a. The black spots in this image are due to mass contrast contributed by multiple overlapping U_2N_3

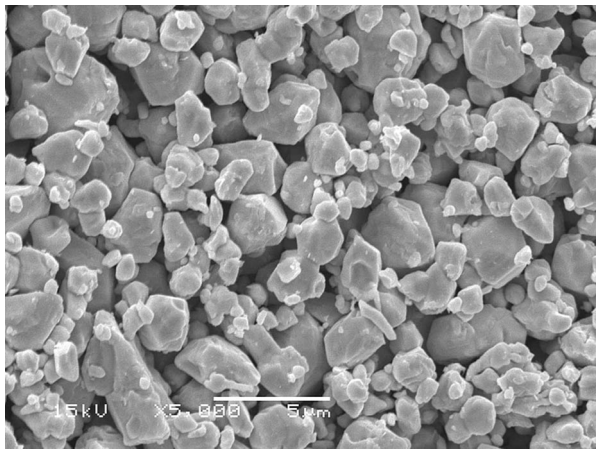

Figure 8. SE-SEM micrograph of UN.

particle layers. Because of these layers, most of the region in the bulk of the TEM BF image is too dense to see a clear picture of U_2N_3 morphology. However, the thickness decreases at the edge of the sample, which allows for quality imaging. No secondary phase precipitates or defects in U_2N_3 are visible in these thin edge areas. The SAD pattern shown in Figure 7b shows the zone axis is along [111]. The weak diffraction spots, as well as some stronger spots possibly corresponding to double diffractions (circled in the image), are due to minor secondary phases (UO_2) and grain overlapping. Grain boundaries can also be observed in the HRTEM image (Figure 7c), which shows lattice fringes in different orientations corresponding to (220) and (422) diffracting planes.

3.5. Microscopy of UN. Particles in the UN sample (Figure 8) appear to have the same size distribution as the UN_2 and U_2N_3 samples. However, the UN particle faces appear noticeably less sharp. While the higher nitride samples show a majority of the larger particles having discrete sharp faces, very few of the similarly sized UN particles have observable flat sharp faces. This observation suggests that either the image is out of focus a little or the UN sample is less crystalline than the higher nitride precursor species.

The TEM BF micrograph in Figure 9a shows several UN particles prepared for imaging by the solution-drop method. Magnified TEM BF images focused on two thin edges, B and C, of one UN particle are shown in Figure 9b and 9c, respectively. The particles shown in this image range from 100 to 150 nm in length, which is in the lower end of the particle size distribution observed in the SEM image. The lack of contrast in the bright field image caused by the high electron scattering factor of UN tends to suppress the detailed structure information, making it difficult to detect the presence of any secondary phases in the BF mode image shown in Figure 9a. However, the magnified images of the selected particles in Figure 9b and 9c show no indication of morphological changes corresponding to a secondary phase. The same two particles in Figure 9b and 9c were used to obtain the HRTEM images shown in Figures 10 and 11, respectively.

The HRTEM image, which was obtained focusing the edge of the particle in Figure 9b, of UN in Figure 10 shows a number of grain boundaries between UN and UO_2 phases.

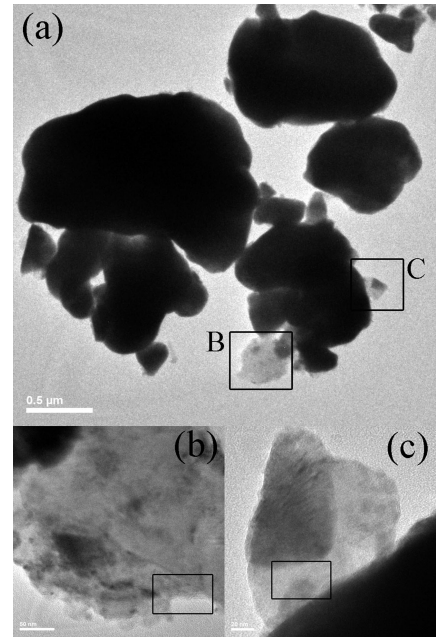

Figure 9. (a) TEM BF image of UN particles embedded on a C−Cu grid using the solution-drop method. (b and c) Magnified particle images corresponding to areas B and C in part a, respectively. Highlighted areas in b and c are used in obtaining the HRTEM images in Figures 10 and 11, respectively.

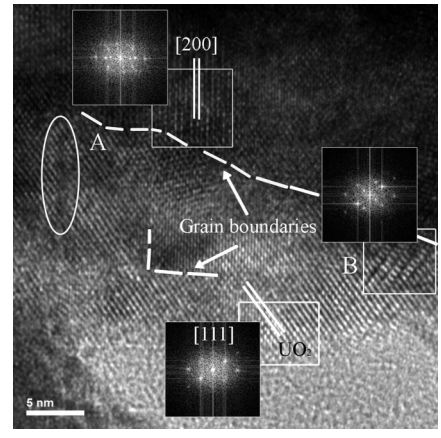

Figure 10. HRTEM image of the highlighted area of the particle in Figure 8b.

UN was identified in the bulk part of the particle, while the lattice fringes near the edge of the particle correspond to the UO_2 phase. The UO_2 phase intrudes 10−20 nm from the edge of the particle into the interior. Most of the particle edge contains details of the UO_2 chemical phase in only one of the [111] directions, and in some patches (area A in Figure 10) the details of the structure is absent. Only one area (area B in Figure 10) contains the fringe details in both directions.

The HRTEM image shown in Figure 11 was obtained by focusing on a thin area of the middle of the particle in Figure 9c highlighted with a box. This image shows no indication of the presence of UO_2 as a secondary phase in this area, supporting the hypothesis that the oxide present in the sample is due to environmental oxidation at the particle surface rather than UO_2 inclusions nucleated within the bulk of the UN phase. The lattice fringes in the image are parallel to the (111) planes of UN structure. Furthermore, the lattice fringes

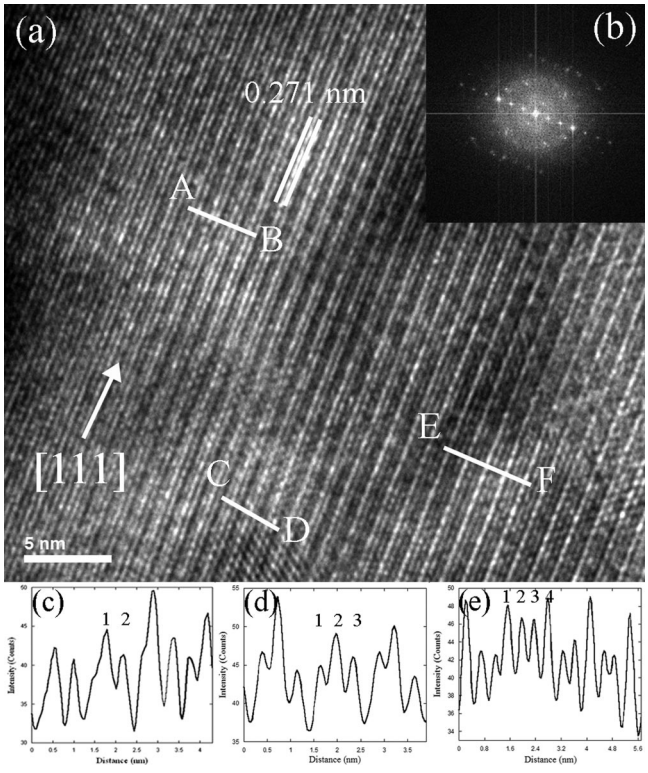

Figure 11. (a) HRTEM image of the particle shown in Figure 8c in the [111] direction and (b) FFT micrograph. (c, d, and e) Intensity profiles of three different regions shown in a denoted by the lines AB, CD, and EF, respectively.

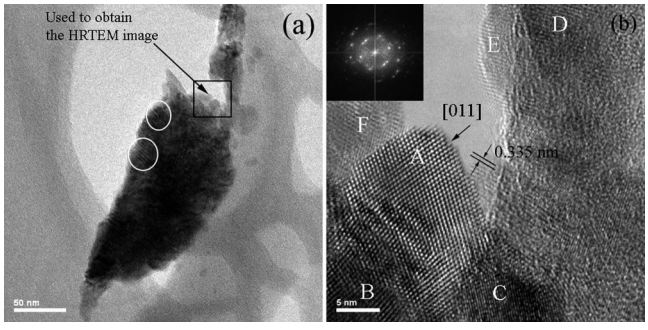

Figure 12. (a) Cross-sectional TEM BF image of a 25 nm thick UN particle prepared using the microtome cutting method, and (b) the HRTEM image obtained. In HRTEM image, the area indicated by A shows both sets of reflections due to (200) UN planes. In all other locations, only one direction of the lattice fringe reflection can be seen. Lattice fringe spacing (0.335 nm) due to UO_2 phase was found at one edge of the particle as indicated.

show a long-range order with different multiplicities of tunnel rows. There are three different tunnel rows: 2-, 3-, and 4-fold. The experimental intensity profiles shown in Figure 11c, 11d, and 11e were obtained along the lattice fringes normal to line segments AB, CD, and EF, respectively. These profiles confirm the tunnel multiplicities (2-, 3-, and 4-fold) of the long-range order in the lattice fringes. The FFT micrograph (Figure 11b) also indicates the presence of well-resolved lattice fringes.

Cross-sectional TEM images of a UN particle that was microtome-cut to a thickness of 25 nm are shown in Figure 12. The particle shown in Figure 12a indicates the presence of some Moiré fringes at the surface of the particle, most

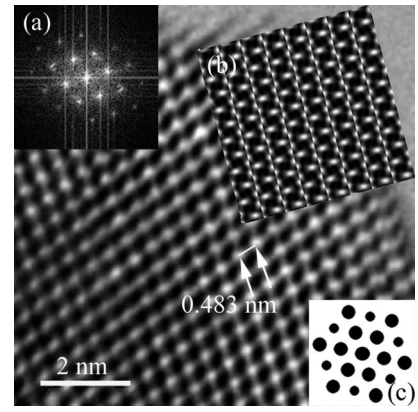

Figure 13. (a) HRTEM image at atomic-level resolution of the UN particle in region A of Figure 12b. Lattice fringes in the HRTEM image correspond to (200) planes of UN in [011] beam direction. (b) Computer-simulated HRTEM image corresponding to $C_s = 1.2$, $C_c = 1.4$, thickness = 25 nm, and defocus = 65 nm. (c) Unit cell image of the UN crystal based on the crystallography of UN in [011].

likely due to the overlapped crystallographic planes of UN with the UO_2 impurity phase. The HRTEM image in Figure 12b was obtained by focusing on the particle area as indicated in Figure 12a. There are a number of grains with lattice fringes in different orientations, confirmed by the FFT micrograph (Figure 12b inset). These regions of different lattice fringe orientation are denoted by letters A−F. Lattice fringes in region A show structure details in all directions of [011] reflections. In all other locations, only one lattice fringe direction can be seen due to the specific grain orientation relative to the microtome-cut surface being imaged. The poorly formed larger-scale fringes observed between locations A and B are likely due to a tilt boundary being imaged roughly parallel to the subgrains. Again, the UO_2 phase can be identified by the 0.335 nm lattice fringe spacing at the edge of the grain.

Figure 13 shows a magnified HRTEM image of region A in Figure 12b. Lattice fringes are parallel to the (200) planes of UN. The calculated HRTEM image (Figure 13b) of UN in the (200) projection with the [011] beam direction using 25 nm thickness and 65 nm defocus value confirms the lattice fringe orientation in the image. Also, considering the orientation of the unit cell determined by the FFT micrograph and a unit cell model (Figure 13c) an approximate value of 0.483(10) nm can be determined for the lattice parameter of UN.

4. Discussion

The XRD patterns of samples produced by the oxidative ammonolysis process showed the UN_2 and U_2N_3 products have high phase purity, with possible contaminations of $UN_{2\pm X}$ incompletely crystallized impurities plus a minimal secondary UO_2 phase due to synthesis equipment or atmosphere. Although the SAD patterns indicated the presence of impurity phases in minimal quantities, impurity levels were below those observable by either TEM BF or HRTEM imaging. It was also found that some of the peaks in the UN_2 XRD pattern can be reduced by heating for longer time periods under NH_3 atmosphere. However, the longer heating time increased the oxide contamination levels, which in turn

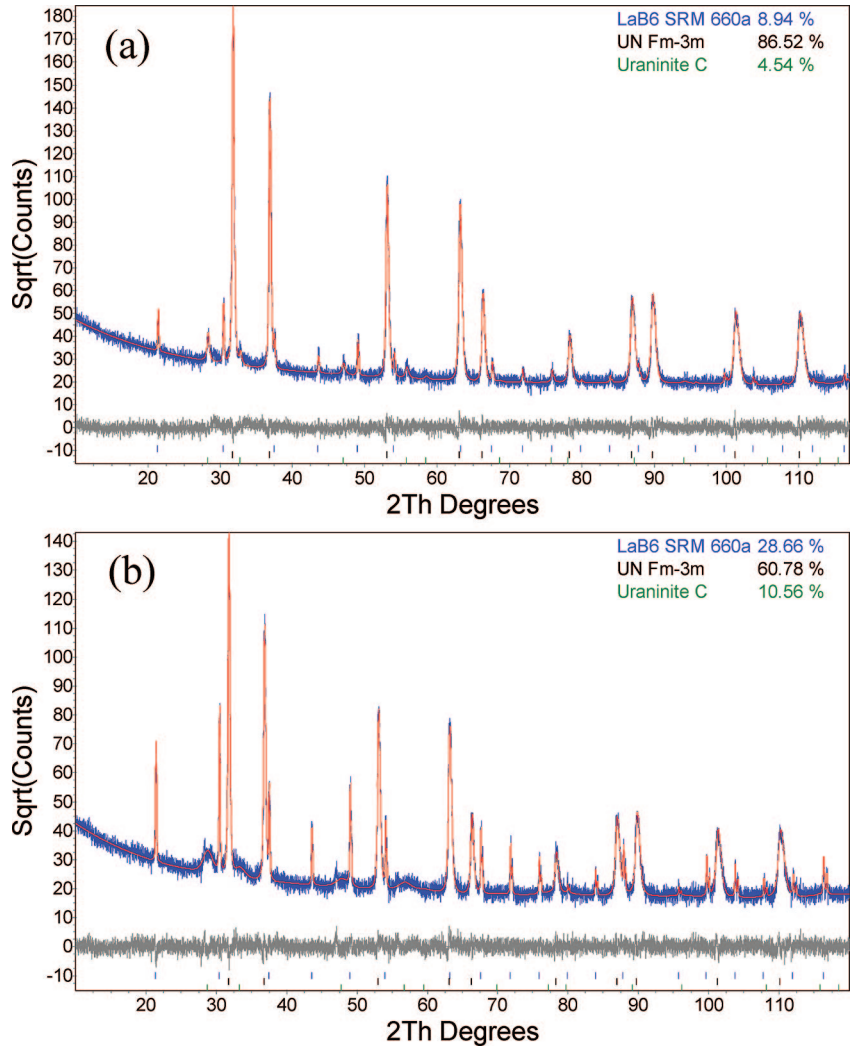

Figure 14. XRD/Rietveld analysis comparison of the UN powder sample: (a) as-synthesized UN, (b) UN sample after 3 months.

would affect the phase purity of the final UN sample using the described synthesis equipment. On the basis of the results obtained through this work, production of high-purity UN does not appear to require reacting the fluoride starting material past the point at which it is fully converted to a uranium nitride, even though the intermediate UN_2 product may be slightly hyperstoichiometric.

HRTEM analysis of the UN samples confirmed that the bulk of the particle consist of UN, as suggested from the XRD pattern, with a UO_2 secondary phase forming on the surface of particles observed (Figures 10 and 12b). The large interior region of the UN lattice fringes, corresponding to the (200) plane (Figure 10), is uninterrupted by UO_2 inclusions. This supports the conclusion that oxide impurities are likely to be formed by a diffusive process from the synthetic environment and thus are also likely to form along the particle surface. Given the high reactivity of UN in any environment not completely devoid of oxygen, contamination from the experimental apparatus is likely to be the source of these oxide impurities rather than the synthetic route. Subsequent analysis of the UN sample after it had been allowed to age for 3 months shows the ingrowth of oxide contamination, lending support to this initial hypothesis. The quantitative analysis performed on the XRD patterns of both these samples showed that the UO_2 level increases from 5.0 (1) to 14.8 (1) wt % over this time period (Figure 14).

Further determination of oxygen impurity levels on the surface of these three samples was done using the XEDS in the STEM mode of TEM. Figure 15 shows the elemental distributions of UN_2, U_2N_3, and UN results determined using XEDS. Uranium and nitrogen are visible in all three samples, but the presence of oxygen in a considerable amount was detected only in the UN sample. Thus, XEDS confirms that the oxide level in the bulk particle area of the analyzed particles is greatest in the UN sample, as found by XRD and electron microprobe.

The stoichiometry between uranium and nitrogen in uranium nitrides is known to be a continuous variable from $UN_{1.75}$ to $UN_{2.0}$ for UN_2 and $UN_{1.45}$ to $UN_{1.75}$ for U_2N_3.[24,25] However, for the lower nitrides the stoichiometry range is smaller, $UN_{0.995}-UN_{0.999}$, than that of the higher nitrides. The refined lattice parameters of UN_2- and U_2N_3-synthesized samples show a match to the reference values only up to the second decimal point (Table 1). The X-ray densities of these two nitrides also vary accordingly. However, the lattice parameter and X-ray density of the synthesized UN matches

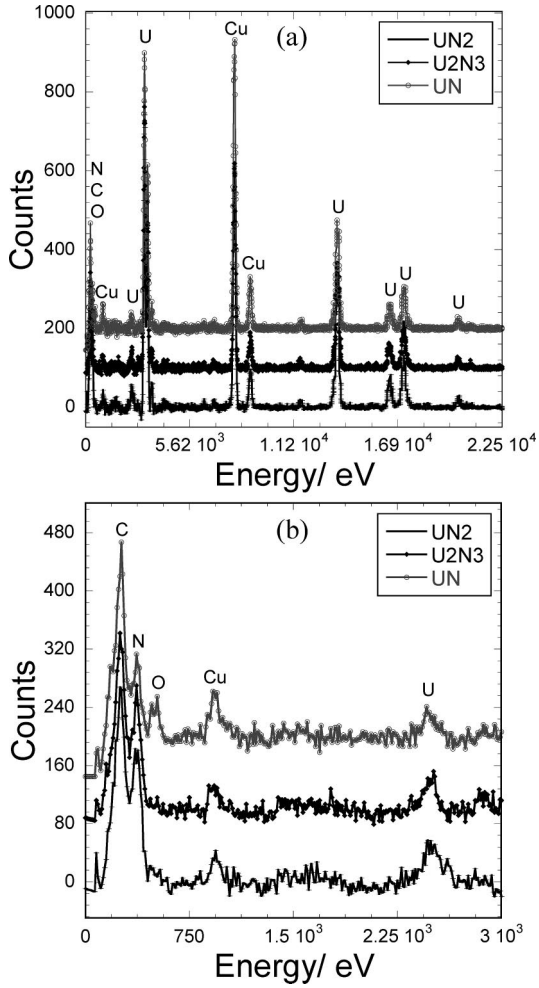

Figure 15. (a) Full and (b) detailed (0.194 > 3000 eV) XEDS spectra of UN_2, U_2N_3, and UN samples; Cu and C peaks are from the sample mounts.

with the reference value within the confidence intervals reported. Thus, the lattice parameter variance in the higher uranium nitrides (UN_2 and U_2N_3) likely indicates the vast range of stoichiometry identified by other authors. The absence of variance in the lattice parameter for the synthesized UN confirms its phase purity to expectations given the narrow range of stoichiometry reported for UN.

As-synthesized uranium mononitride particles appeared to fall within a particle size distribution of 0.1–6 μm. Furthermore, the particle sizes estimated by SEM were verified by TEM. This particle size range is consistent with the previously reported microscopic data,[16] and it is similar to the particle size distribution observed for the UN_2 and U_2N_3 precursor phases. The surface area measurements of the nitride species also show no significant change as the UN_2 is converted to the U_2N_3 and UN products, suggesting that conversion of the higher nitrides to the mononitride does not significantly impact particle size or morphology.

5. Conclusion

Uranium nitrides synthesized using the oxidative ammonolysis of UF_4 were successfully characterized by means of XRD, electron microscopy, and surface area analysis. For the first time, TEM BF and HRTEM techniques were applied in morphological and microstructural observations of UN_2 and U_2N_3. The UN samples synthesized from UN_2 contained measurable levels of UO_2, as high as 5.0 (1) wt %. The change in surface area for the uranium nitride species was minimal, with an order of magnitude increase in surface area observed from the initial fluoride species.

The TEM observations of this UN sample showed that UN has long-range order in its microstructure. Furthermore, the HRTEM images of microparticle surface and cross-section made by solution-drop and microtome-cutting methods, respectively, showed the secondary oxide phase formed primarily on the UN particle surface. Given the absence of an oxide phase in the UN_2 and U_2N_3 samples in large quantities, oxide contamination appears to form during the final stage of the process, most likely due to oxygen contamination in the experimental system used for this synthesis. Observed increases in uranium oxide levels in UN after long-term exposure to air support the conclusion. Better oxygen control during the final decomposition reaction, such as replacement of the quartz furnace tube and addition of oxygen getters for the cover gas, may be sufficient to reduce the oxide levels within the UN product as well as storage of the UN samples under inert atmosphere. This would allow for production of sintered UN pellets and testing of the sinterability of UN from this synthetic route.

Acknowledgment. The authors wish to thank Dr. Anthony Hechanova for administrating the UNLV Transmutation Research Program under the financial support of the U.S. Department of Energy (Grant No. DE-FG07-01AL67358). We also thank Drs. Clay Crow and Robert Fairhurst, from the Department of Geoscience at UNLV, for helpful discussions and support. The authors are indebted to Tom O'dou and Trever Low for laboratory management and radiation safety.

CM7033646